11th ANKARA INTERNATIONAL AEROSPACE CONFERENCE   **AIAC-2021-055**
8-10 September 2021 - METU, Ankara TURKEY

EVALUATION OF VARIOUS DESIGN OPTIONS FOR WING LEADING EDGE AGAINST BIRD STRIKE

Muhammet Cihan TEZEL[1], Yusuf YAMANER[2], Erdem ACAR[3]   Bilge Aziz ÇOĞUZ[4]
TOBB University of Economics and Technology   Turkish Aerospace
Ankara, TURKEY   Ankara,TURKEY

ABSTRACT

This study investigates the effects of bird strike to the wing leading edge of a trainer aircraft in accordance with the EASA CS-23 standards, and compares various options for design of energy absorbing support structures. In this study, bird models with hemispherical-ended cylindrical geometry are simulated using the Smooth Particle Hydrodynamics (SPH) finite element approach. After validating the impact of the bird model with a rigid plate, the bird strike on the wing leading edge is modelled, and the results are compared with the existing experimental and simulation data available in literature. Finally, different design options for support structures of the wing leading edge are evaluated and the results are compared. It is found that honeycomb sandwich panel support structure displays the best collusion and weight performance.

Keywords: Bird strike analysis, Wing leading edge, Smooth Particle Hydrodynamics (SPH) method, Honeycomb, Triangular reinforcement structures

INTRODUCTION

The collision of aircraft and birds affects flight safety, causes financial losses and loss of lives. Aviation authorities such as the Federal Aviation Administration (FAA) and the European Aviation Safety Agency (EASA) published regulations to reduce the effects of accidents and ensure flight safety. According to crash reports and statistics, windshield, radome, engine, wings and empennage are the areas damaged by birds [Metz, 2020]. To ensure that the aircraft structures are resistant to bird strikes, experimental tests are carried out on the aircraft structural parts most affected by the impact. The repetition of experimental testing, the reproduction of leading edge structure and development of designed parts are costly and time-consuming processes. Due to their low computational cost and high accuracy, numerical simulations are used to analyse bird strike problem.

---

[1] BSc. Student in Mechanical Engineering Department, Email:mtezel@etu.edu.tr
[2] BSc. Student in Mechanical Engineering Department, Email:yyamaner@etu.edu.tr
[3] Professor in Mechanical Engineering Department, Email: acar@etu.edu.tr
[4] Senior Design Engineer, Turkish Aerospace, Email:bcoguz@tai.com.tr

To examine the bird strike problem in detail, the behavior of the bird at the time of impact should be examined. In the experimental studies of Barber and Wilbeck [Barber and Wilbeck, 1975], the impact of the bird on a rigid plate was investigated. The impact pressures on the bird were determined. With the development of computers and the decrease in calculation costs, simulation based studies have been widely used to solve bird impact problems. Lavoie [Lavoie, 2009] compared an experiment of impinging the gelatin bird model to the plate with the crash model generated in LS-DYNA.

Light weight and high strength are important design criteria in aviation. Various support structures have been designed to reduce the effects of bird strikes at the wing leading edges. Innovative designs such as sandwich panels and triangular reinforcement structures have been used along with the newly developed materials and production technologies. In the study of Liu [Liu, 2017] honeycomb and foam support structures were compared in terms of their crash performance, and it was found that honeycomb had a better crash performance. Di Caprio [Di Caprio, 2019] used a numerical model to examine collision-resistant leading edges with different core configurations and different thicknesses in honeycomb structures. The results showed that thicker honeycomb structures and thicker shells were the best solution to reduce deformation by absorbing the high energy generated in bird strike. Arachchige [Arachchige, 2020] compared honeycomb and foam sandwich panel structure at the composite leading edge. Hanssen [Hanssen, 2006] conducted experimental and numerical simulations against bird strikes on foam-based aluminum sandwich panels. This model was used to determine the minimum foam thickness that can handle bird strike effects. Smojver [Smojver, 2010] modeled the impact behavior using sandwich panels formed by composite and Nomex honeycomb structures on the wing edges. Besides sandwich structures, Liu [Liu, 2017] introduced triangular reinforcement elements as an innovative design, compared the triangular reinforcement elements produced with different design techniques, and confirmed their simulation results through experiments.

The main objective of this paper is to evaluate different design options for support structures of the wing leading edge through finite element analyses, and determine the best design option in terms of both crash and weight performance. The remainder of the paper is organized as follows. Section 2 presents the models used in the analysis of the bird strike against wing leading edge of a trainer aircraft and provides an overview of these models. Section 3 presents the validation studies conducted for the bird model as well as the leading edge finite element model. The finite element modelling of various support structures of the wing leading edge explained, and their impact performances are compared in Section 4 to arrive at an optimal design option with the best crash and weight performances. Finally, the paper culminates with the concluding remarks listed in Section 5.

METHOD

In this study, bird strike on the wing leading edge of a trainer aircraft is analysed by the combined use of three models: (i) the bird model, (ii) the wing leading edge model, and (iii) energy-absorbent support structure model. The flowchart shown in Figure 2 is followed during the simulation of bird strike on the wing leading edge. Brief details of each model are provided in the followings.

The bird model includes finite element modelling, equation of state modelling, bird geometry construction, and determination of proper hourglass and viscosity parameters. As shown in Fig. 3, the soft body impactor of the bird in high-speed impact allows the use of Lagrangian, ALE (Arbitrary Lagrangian Eulerian), Eulerian and SPH (Smoothed Particle Hydrodynamics) as the method for the FEM solution [Dede, 2015].

In various studies, Lagrange, ALE and SPH methods were used in bird strike problems and these three methods were compared. Studies stated that the Lagrange method does not give reliable results at high deformations, the ALE method causes high computational costs, and the SPH method is preferable because of its smaller computational cost compared to ALE Method. In addition, according to experimental and simulation behaviour of the bird, the SPH

method has the closest result. [Anghileri, 2005; Castelletti, 2003]. Different studies in the literature also prefer SPH method [Guida, 2011; McCallum, 2005].
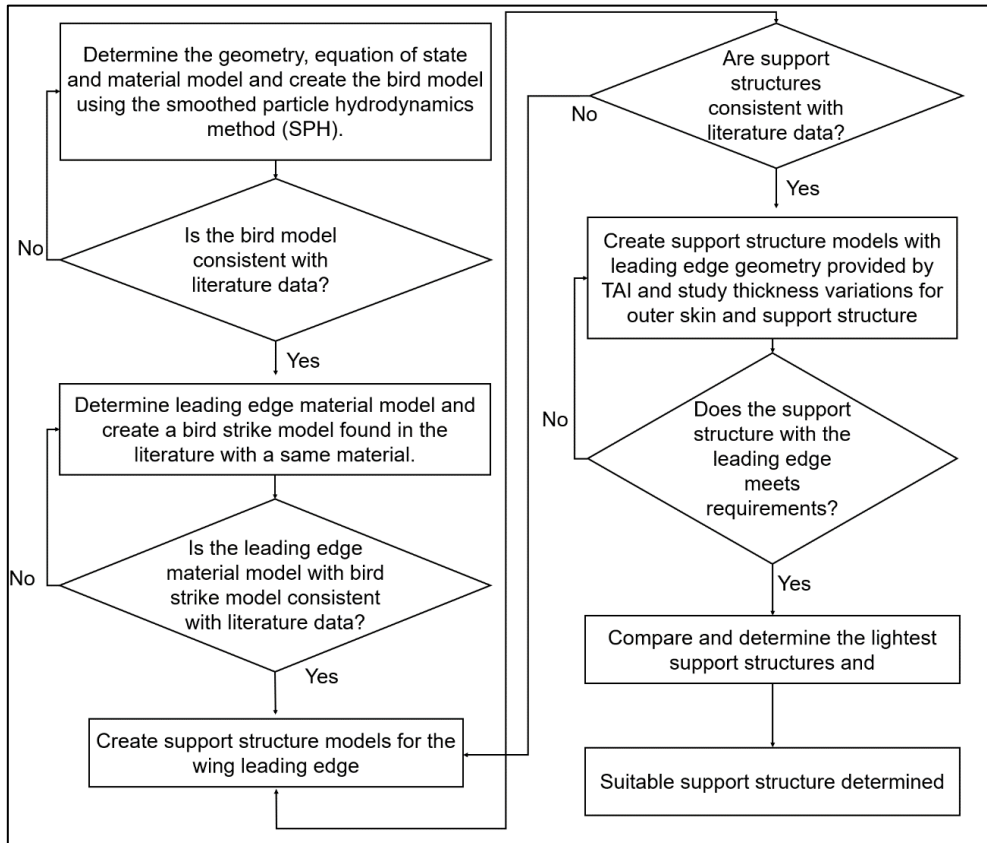

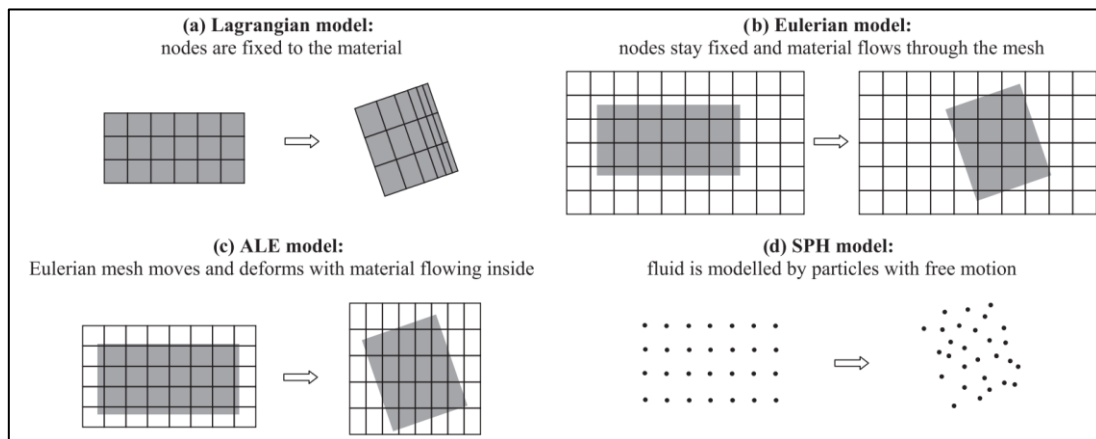Figure 1: Flowchart of bird strike against wind leading edge analysis

Figure 2: Different finite element approaches a) Lagrangian b) Eulerian c) ALE d) SPH approaches [Heimbs, 2011]
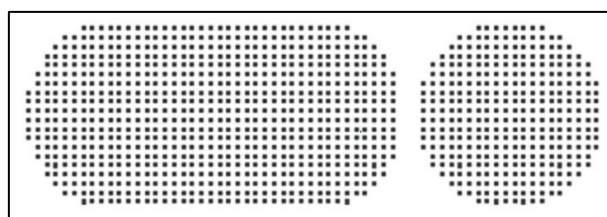

Figure 3: Hemispherical-ended cylinder bird model in two views created with SPH method

Cylinder, spherical and hemispherical-ended spherical geometries are widely used in literature to simplify the bird geometry. It was found that the hemispherical-ended cylinder bird model has the closest impact behaviour to the natural bird behaviour [Johnson, 2003; Nizampatnam, 2008]. Consequently, SPH method with hemispherical-ended cylinder shown in Fig. 3 is used for modelling the bird, in this study.

Due to high-velocity impact, bird's deformation is considered under four different categories as elastic, plastic, hydrodynamic and explosion. As the internal stresses exceed the strength of the skin material, the hydrodynamic zone transition causes it to behave like a liquid [Hedayati, 2015]. Accordingly, birds are modelled as a mixture of water and air. To determine the hydrodynamic response of the fluid, an equation of state (EOS) is required to accurately simulate material behaviour. An EOS determines the hydrostatic behaviour of the material by calculating pressure as a function of density [LSTC, 2007]. EOS-Gruneisen, EOS-Linear Polynomial and EOS-Tabulated can be used to model the bird strike on the leading edge. In this study, we use EOS-Linear Polynomial for bird model.

To validate the bird model, the results of pressure profile, velocity profile and dispersion of the bird on the plate are compared with the existing studies in literature. When the bird hits the target, a high pressure occurs on the bird, called the Hugoniot pressure. In Fig. 4, the peak value in zone A corresponds to the Hugoniot pressure. In Fig. 4, zone A is called the initial shock regime, zone B is named as pressure decay regime, zone C is named as steady-state regime, and zone D as named as pressure termination regime [Hedayati, 2014].
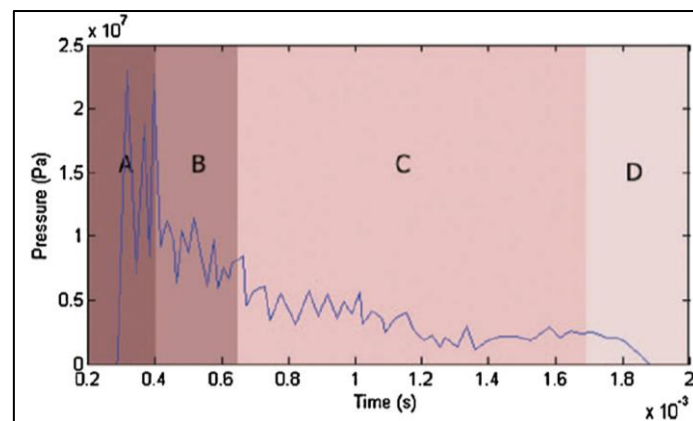

Figure 4: Experimental pressure profile for a bird striking a rigid target for the bird initial velocity of 116 m/s [Hedayati, 2014]

Bird strike on the wing leading edge results in plastic deformations, and failure may occur on the leading edge. Several material models can simulate the deformations caused by bird strike, such as Steinberg material model, Mechanical Threshold Stress (MTS) material model, Johnson Cook material model and piecewise linear plasticity material model [Dede, 2015]. In addition to these models, the isotropic elastic–plastic model (3-MAT_Plastic_Kinematic) and the continuum damage mechanics (CDM) model, which includes anisotropy and viscoplasticity (MAT_damage_1) are also used in the literature [Guida,2008; Hanssen, 2004].

To make wing leading edges more resistant to bird strikes, support structures such as sandwich panels and triangular reinforcement structures are used. Various configurations for honeycomb sandwich panels on the C27-J aircraft wing leading edge have been tested and achieved success [Guida, 2008; Belkhelfa, 2020; Di Caprio, 2019]. As a different study, triangular reinforcement structures examined to bird resistant the tail leading edge against bird strike [Liu, 2017].

In this study, the impact performances various energy-absorbent support structures, that will be integrated to the wing leading edge, is evaluated. The obtained designs should satisfy the EASA CS-23 test standards as well as the TAI's requirements. EASA standards state that

successfully completing a flight after an impact with a 2 lb bird when the aircraft's velocity relative to the bird along the aircraft's flight path equals cruise speed which is 270 knot. In addition, TAI's requirements for the wing leading edge design is that no critical damage to the front spar elements or the wing tank, assuring a continued safe flight and landing after impact. In addition to all these requirements, with a conservative approach, the scenario where the bird do not contact the front spar element were considered successful.

VALIDATION STUDIES

Validation of the bird model

In literature, bird strike on a rigid plate was analysed by using FE method, and compared with experimental data [Lavoie, 2009]. In that experiment, 1 kg of bird was impacted at a speed of 100 m/s on a fixed plate of 0.305 x 0.305 m^2 and 0.0127 m thickness. Plates in the experiments were fixed from the edges. In the experiment, the speed of the bird thrown at 100 m/s was measured as 95 m/s during bird contact the plate. Therefore, the bird velocity in the numerical study was taken as 95 m/s. For the bird with a mass of 1 kg and a density of 950 kg/m^3. The hemispherical-ended cylindrical bird has 93 mm diameter and 186 mm length. In Fig. 5, snapshots of the experiment performed with the gelatine bird model and the numerical analysis are given at 0.66 ms intervals from the moment of collision.
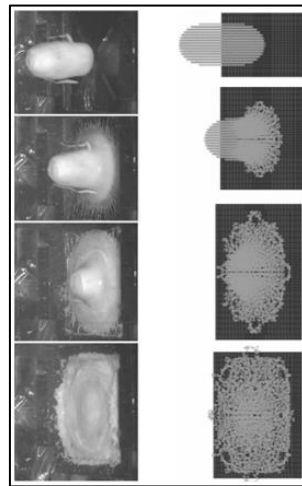

Figure 5: Bird Strike Experiment and Numerical Analysis [Lavoie,2009]

In this study, 10000 hexahedral solid finite elements are used to model the plate and 4836 particles are used to model the bird. The number of elements and particles are similar to those of the Lavoie (2009). The plate thickness is 0.0127 m. In this study, first a hemispherical cylinder geometry with a diameter of 0.093 m and a length of 0.186 m was first assigned to a shell element. Subsequently, SPH particles are created over this shell element. SPH generation stage and SPH particle distribution are given in Fig. 6. Bird strike analysis models are given in Fig. 7.
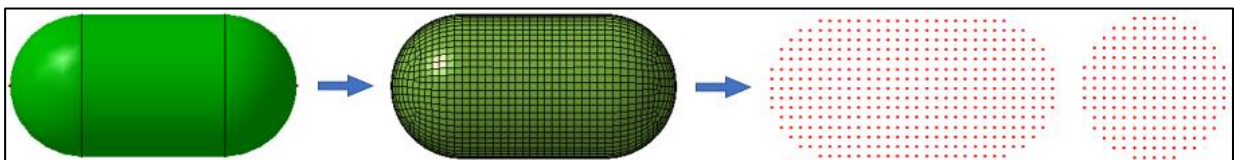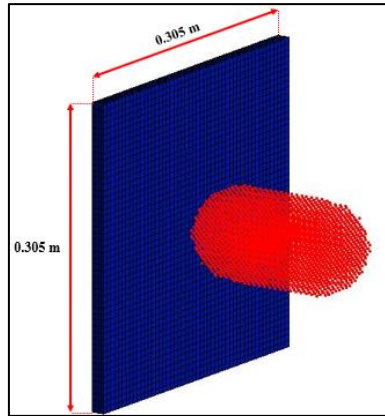

Figure 6: SPH Generation and Particle Distribution

Figure 7: Numerical Model of Bird Strike Analysis

The material properties are taken from Lavoie's (2009) study. The target plate is rolled homogeneous armour steel (RHA steel). MAT_ELASTIC material card is used for the material. Its density is 7830 kg/m³, its elastic modulus is 207 GPa and the Poisson's ratio is 0.3.

MAT_ELASTIC_PLASTIC_HYDRO is used as material card for bird and EOS_LINEAR_POLYNOMIAL is used as state equation card. In the material card, the density is 950 kg/m³, the shear modulus is 2 GPa, the yield strength is 20 kPa, the plastic hardness modulus is 1 kPa and other parameters are 0. In the equation of state card, the parameters are assigned as C0 = C4 = C5 = C6 = 0, C1 = 2.06 GPa, C2 = 6.19 GPa, C3 = 10.3 GPa.

Q1 (quadratic viscosity coefficient) = 2 and Q2 (linear viscosity coefficient) = 0.25 are used in the CONTROL_BULK_VISCOSITY card. IHQ (hourglass viscosity type) = 2 and QH (hourglass coefficient) = 0.14 are used in the CONTROL_HOURGLASS card.

The CONTACT_AUTOMATIC_NODES_TO_SURFACE card is used to define the contact between SPH particles and solid elements in the analysis. FS and FD are the static and dynamic coefficient of friction between the bird and the plate and they are both assigned as 0.2. SPH particles are defined in SSID (slave segment set ID) and plate IDs in MSID (master segment set ID).

Figure 8 shows a comparison of the pressure readings at the point where the center of the bird strikes hits the rigid plate at 0°. It is observed that the numerical results of this study are consistent with both the numerical and experimental results of Lavoie (2009) in terms of the behaviour of the steady state pressure region and Hugoniot pressure.
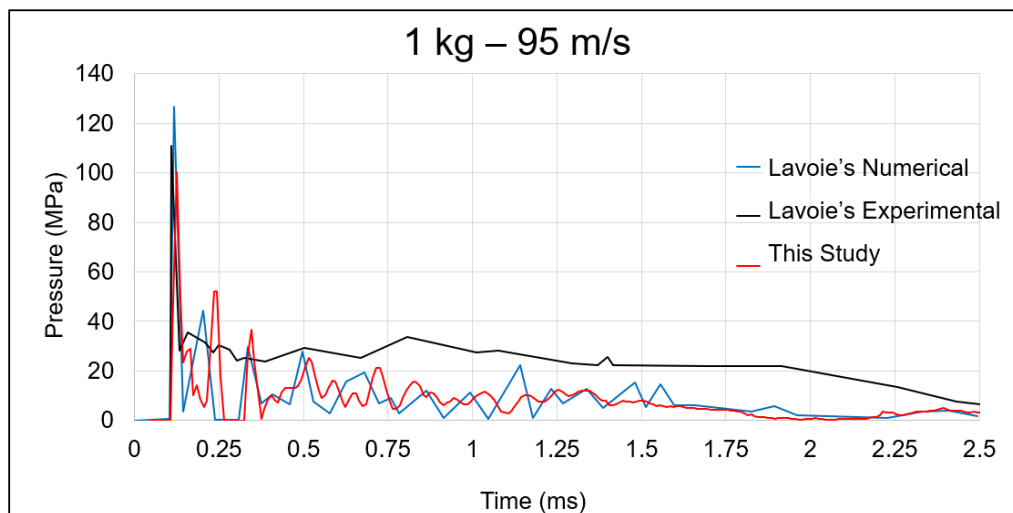

Figure 8: Pressure readings (experimental vs. numerical)

Figure 9 shows the variation of velocity and diameter of projectile at 0º for the experimental results and numerical models. It is observed that the results of the numerical model of this study are consistent with numerical model of Lavioe (2009), and both numerical models provide close results with respect to the experimental data.
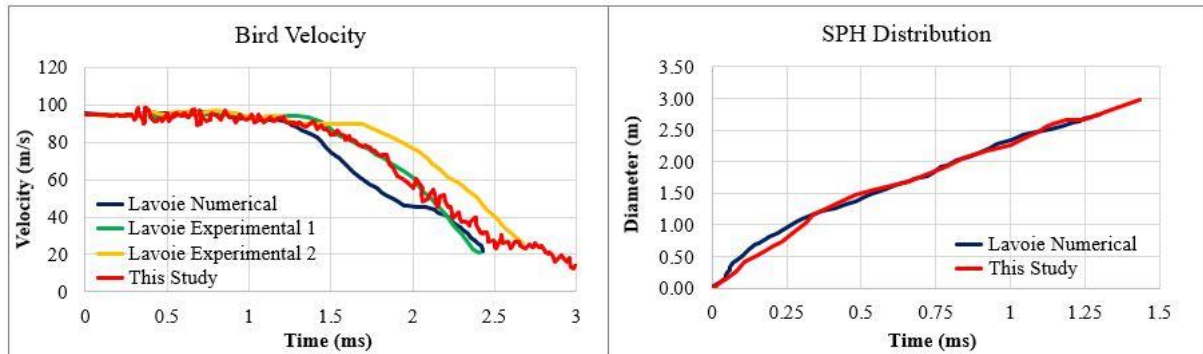

Figure 9: The variation of velocity and diameter of projectile at 0º

Validation of Leading Edge Model

For the validation of the wing leading edge model, study of Guida (2011), which compared the experimental and the numerical leading edge model, is selected. Guida conducted a bird strike analysis in the tail of the C27J aircraft according to FAR 25.631 regulation. The tail model and dimensions used in the experiment are shown in Fig. 10. According to the regulation, the bird mass must be 8 lb (3.68 kg) and must be occurred at 129 m/s on the tail leading edge.
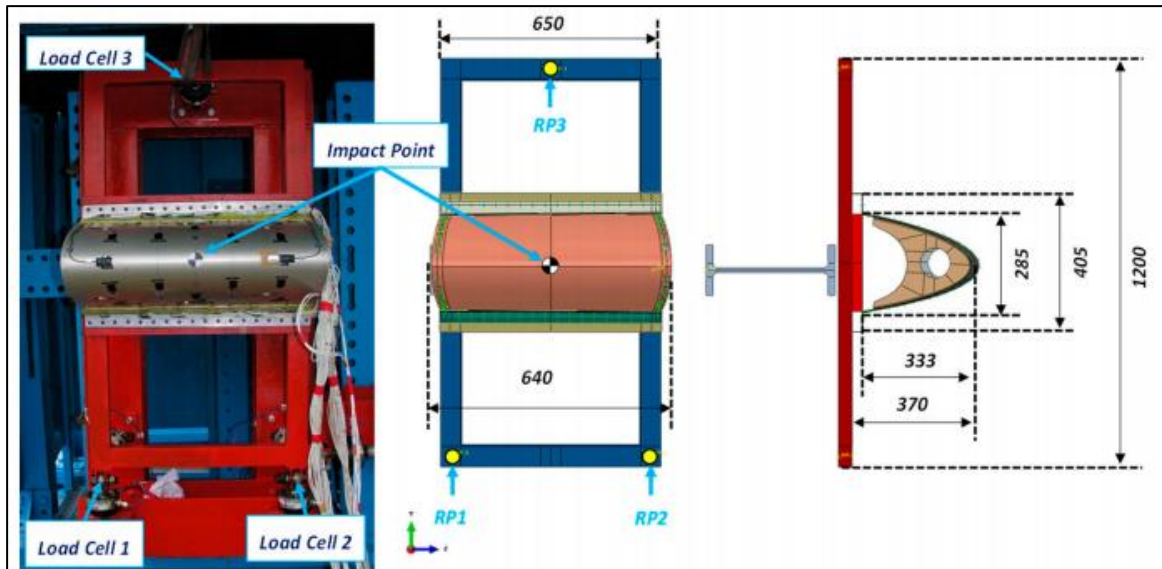
Figure 10: Guida's Wing Leading Edge (dimensions are in mm)

Guida's study is includes various different configurations of skin and honeycomb thicknesses as well as materials. In this study, the configuration that consists of 1.4 mm thick AA 2024 outer skin, 6.35 mm Hexcel Flexcore honeycomb, and 0.4 mm thick AA 2024 inner skin. This configuration is selected since it was the one closest to the wing leading edge that are considered in this study.

In Guida's study, the bird model was created by modelling the cylinder geometry with the Lagrange method and the analyses were made in the MSC / Dytran finite element program. The finite element model of the bird and tail Leading edge is shown in Fig. 11.
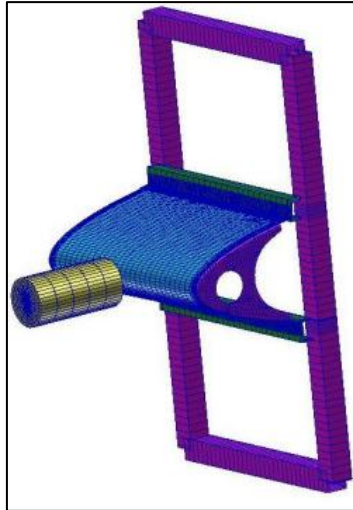
Figure 11: Guida's Numerical Model

In this study, LS-DYNA is used to predict the effects of bird-strike on the leading edge. The leading edge finite element model consists of two beams, two ribs, outer skin, honeycomb and inner skin. The beams, support elements, front surface and inner surface are formed by 4 node shell elements. The honeycomb structure is composed of 8 node solid brick elements. The beams and ribs are 2 mm thick, the outer surface is 1.4 mm, the inner surface is 0.4 mm and honeycomb are 6.35 mm thick. The inner and outer surfaces consist of 4928, beams 845, support structures 1006 elements, and overall, there are 11707 shell elements in total. 4928 solid elements are used to model the core structure. Beams, support elements, outer and inner surface material AA 2024 T3. The finite element model of leading edge is shown in Fig. 12.
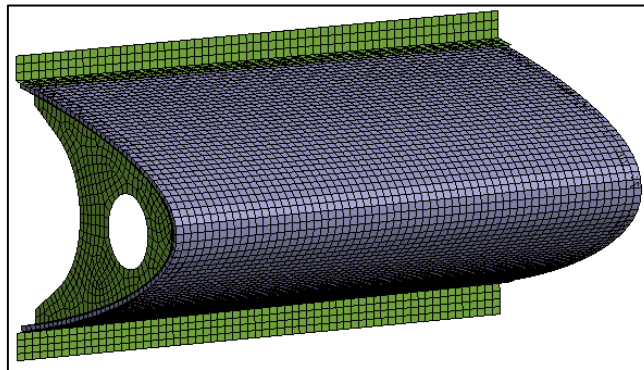
Figure 12. Wing Leading Edge Finite Element Model

Cylinder geometry is used to be similar to the study to be validated in the bird model. The bird model with a density of 946.6 kg/m^3 is 134 mm in diameter and 268 mm in length, and its mass is 3.679 kg. The SPH method is used as the finite element method and there are 12640 particles. The SPH particle distribution is shown in Fig. 13. All parts in the analysis have a total of 29275 elements.

Figure 13. SPH Particle Distribution

The bird model cards, which are validated in the previous section, are used as the bird material and state equation card. MAT_DAMAGE_1 material model is used for AA2024 T3 material and parameter information is taken from Hanssen's [Hanssen,2006] study. Density 2.77×10^{-3} g/mm^3, elastic modulus 73.08 GPa, Poisson's ratio 0.33, yield strength 334 MPa.

MAT_MODIFIED_HONEYCOMB material model is used for the honeycomb support structure. Density 4.6×10^{-5} g/mm^3, fully compressed material elastic modulus 0.9 GPa, Poisson's ratio 0.34, yield strength 35 MPa, breaking volume 0.15, elastic modulus $E_{11} = E_{22} = 10$ MPa, $E_{33} = 861$ MPa, shear modulus $G_{12} = 10$ MPa, $G_{13} = 200$ MPa, $G_{12} = 90$ MPa. Stress strain graph is defined to LCA with DEFINE_CURVE card. The stress-strain graph is given in Fig. 14.
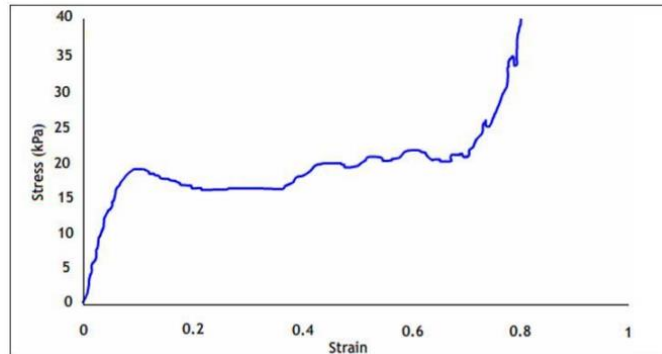
Figure 14. Honeycomb Stress-Strain Graph [Guida, 2008]

The CONTACT_AUTOMATIC_NODES_TO_SURFACE card is used to define the contact between the SPH particles and the wing surface. Due to a possible puncture situation, the contact card for each layer of the surface with SPH particles is defined.

CONTACT_AUTOMATIC_SINGLE_SURFACE contact card is used since the wing surface, rib elements and beams are compressed after the bird hits the wing surface. When the structure is deformed, contact occurs as a result of the folds within itself. In order for the deformed structure to deform itself, single surface contact algorithm is given.

Surface to surface contact algorithm used to show the effect of deformed elements on each other. After the bird impact the outer skin, the outer skin undergoes deformation. During deformation, skin contacts other elements such as beam. CONTACT_AUTOMATIC _SURFACE_TO_SURFACE contact card was used to deform the beam as a result of the contact of the outer skin. The outer surface that causes deformation in contact is defined in the SSID (slave segment set ID), and the beam is defined in the MSID (master segment set ID).

The relationship of the parts connected to each other by mechanical assembly is defined by the CONTACT_TIED_SURFACE_TO_SURFACE contact card. The outer surface is connected to the beams, the support structure to the outer surface, the inner surface to the supporting structure and the support elements to the inner surface.

The center displacement on the leading edge and displacement on the ribs between the experimental test and numerical model were examined in the study. Figure 15 shows that the change of the center point in the collision zone over time, and the results of this study are close to those of Guida [Guida, 2009]. Figure 15 also shows that the maximum displacement value is consistent with the 350 mm value measured as experimental result. Figure 16 depicts that the variation of the displacement of edge ribs over time is also consistent with the results obtained by Guida. Finally, Figure 17 shows that the post-collision deformation of the ribs and wing deformations obtained in this study are also consistent with the results obtained by Guida.
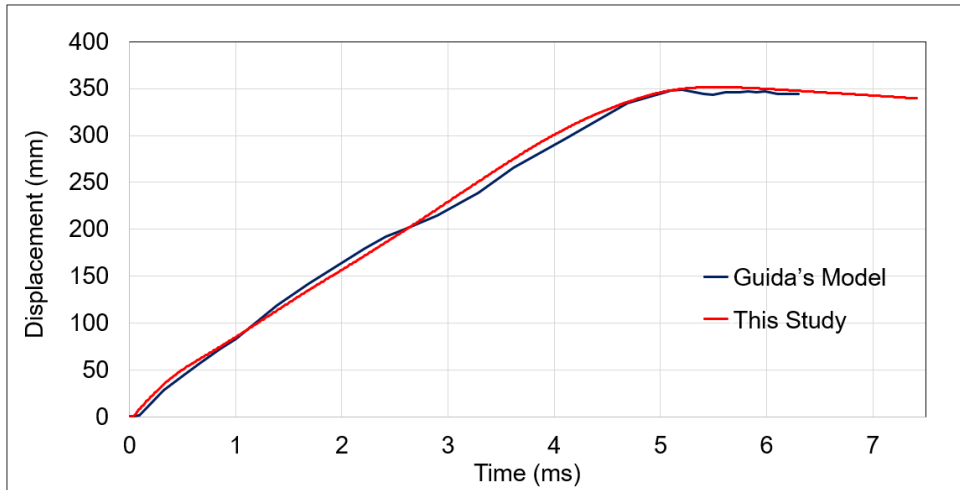
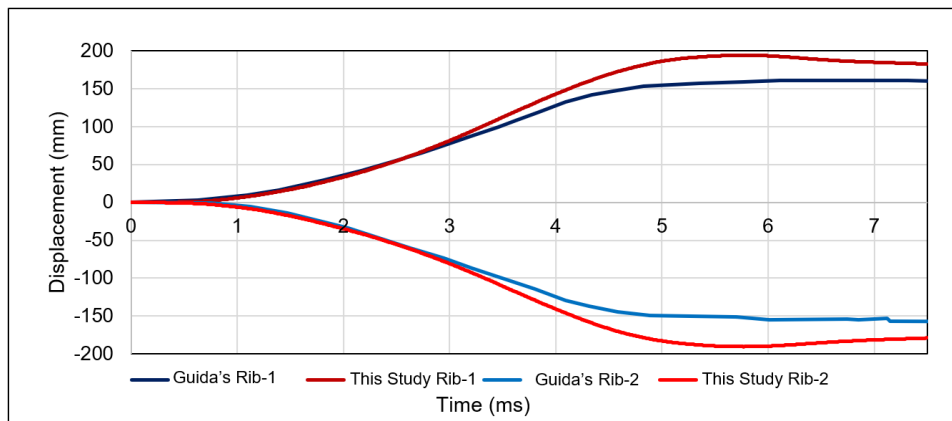Figure 15: Displacement of Center Node
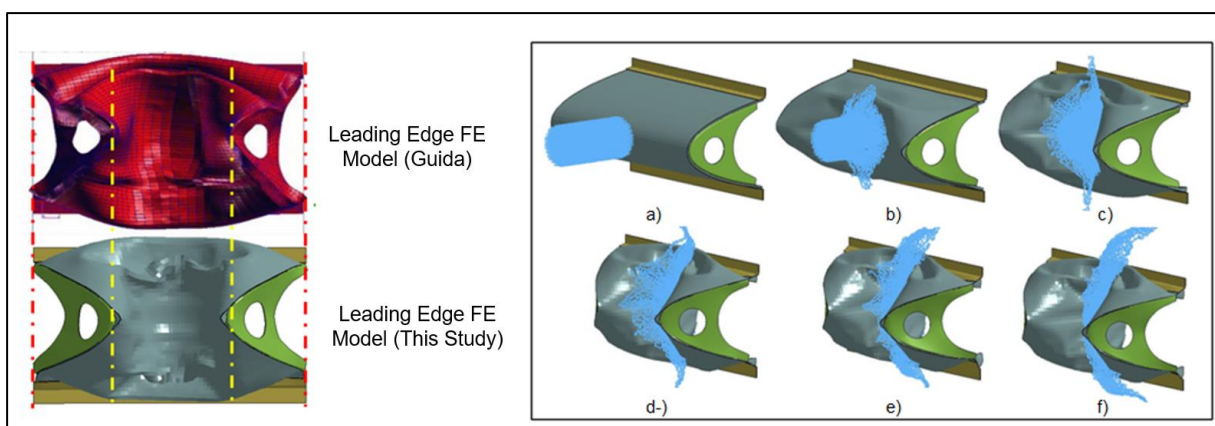

Figure 16: Displacement of Edge Ribs

Figure 17: Deformation comparison between leading edge FE Model and impact sequence with 1.5 ms intervals at $t_a = 0$ ms

APPLICATION STUDY

After validating our bird model and the wing leading edge model, we apply our modelling abilities on our specific application study. In this application study, the wing leading edge geometry provided by TAI is used (see Figure 18). According to TAI's wing structural design experiences, the proper range of thickness value for outer skin is between 1.0 and 1.6 mm. The wing skin material is AA 2024 T3, the front spar material is AA 2024 T42. The thickness of the front spar is 2 mm. In this study, the leading edge design is assumed to be successful if there is no contact on the front spar element after the impact. This success criterion is based on the CS-23 requirements and TAI's wing design practices. It is noteworthy that that in addition to this impact performance requirement, minimize the wing mass is investigated.
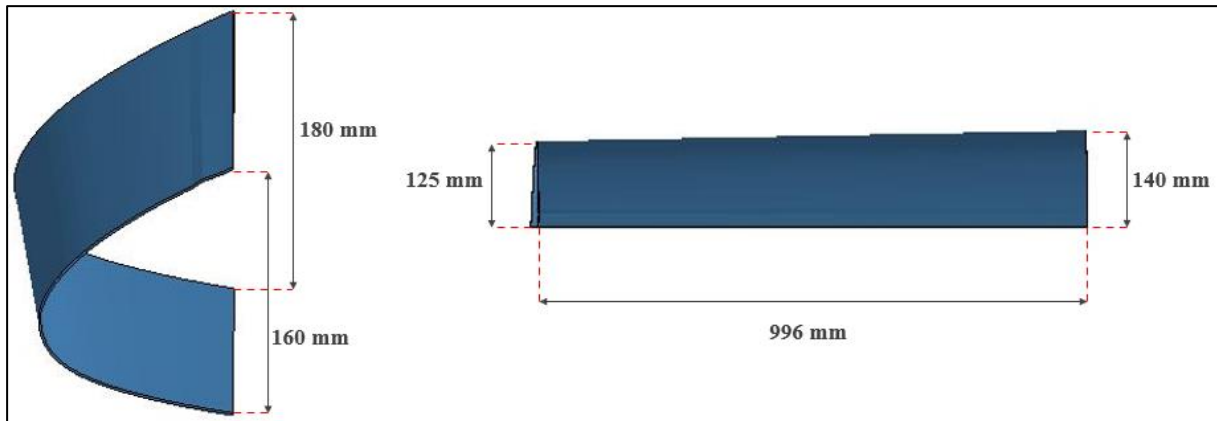
Figure 18: Wing Leading Edge Geometry

Boundary Conditions

3-DOF displacement constraints are used at the beginning and end points of the wing sections. 6-DOF displacement and rotation constraints are used in the parts of the front spar that connect with the body elements. Boundary conditions are shown in Figure 19.
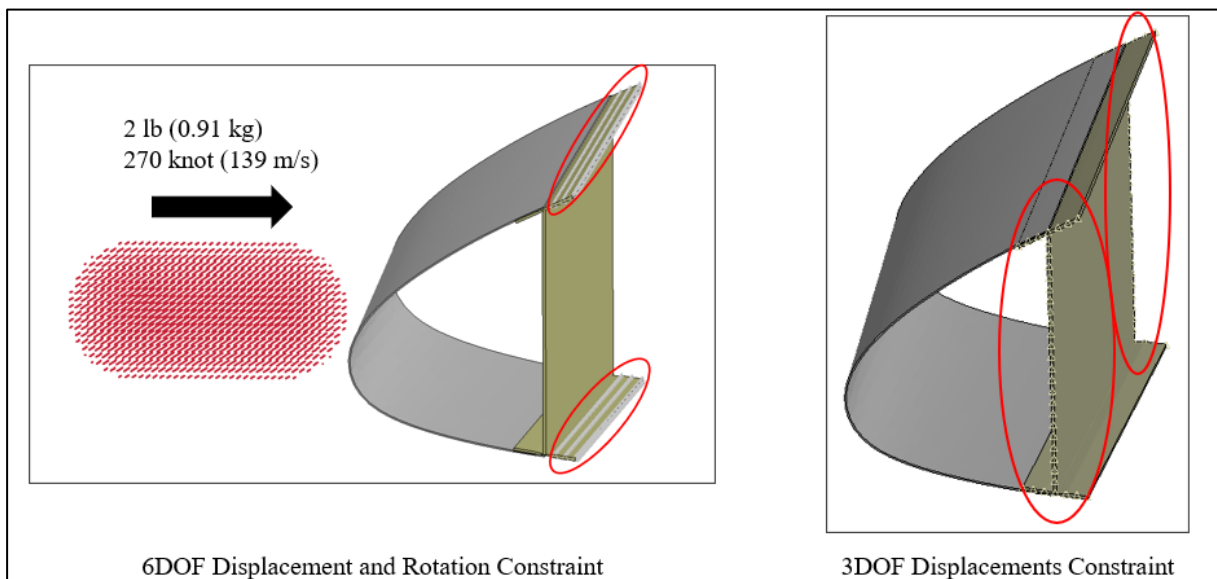

Figure 19. Boundary Conditions

Leading Edge Configurations

Outer Surface Only: "Outer Surface Only" configuration is aimed to determine the thickness that the outer surface can withstand against bird strike when there is no additional support structure. In this configuration, different outer skin thickness values between 1.6-2.0 mm are analysed. The material of outer skin is used AA 2024 T3. The minimum thickness value satisfying CS-23 requirements is found as 1.85 mm. Figure 20 shows only the outer surface configuration.
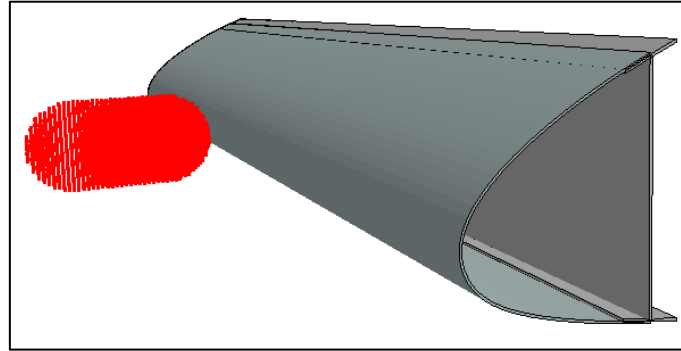

Figure 20. Only Outer Surface

Traditional Rib Design: "Traditional Rib Design" configuration is created to explore the behaviour of the classical design used in certifications. The material of the ribs is AA 2024 T3. There are 6 ribs on the wing leading edge part analysed. Each rib is 200 mm apart from each other. The rib thickness is 2 mm, and the ribs are 20 mm wide. Two different collision scenarios in the impact zone have been examined. In the first condition, the bird is impacted directly on a rib. In the second condition, the bird is impacted middle of two ribs. Traditional rib configuration is shown in Figure 21.
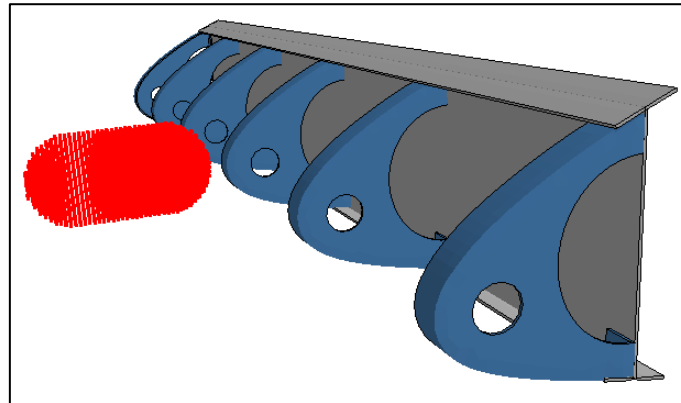

Figure 21: Traditional Rib Design

Honeycomb Structure: In this configuration, "HexWeb Aluminum 5052 Flex-Core, 6.35 mm" product of Hexcel company is used. AA 2024T3 is used as inner and outer panel material. In this configuration, the thickness of the outer skin is 1.2 mm, the honeycomb thickness is 6.35 mm, and the inner skin thickness is 0.4 mm. The mounting interface is used for to mount the panels to front spar element. The mounting interface is made of AA 2024 T3. Honeycomb structure configuration is shown in Figure 22.
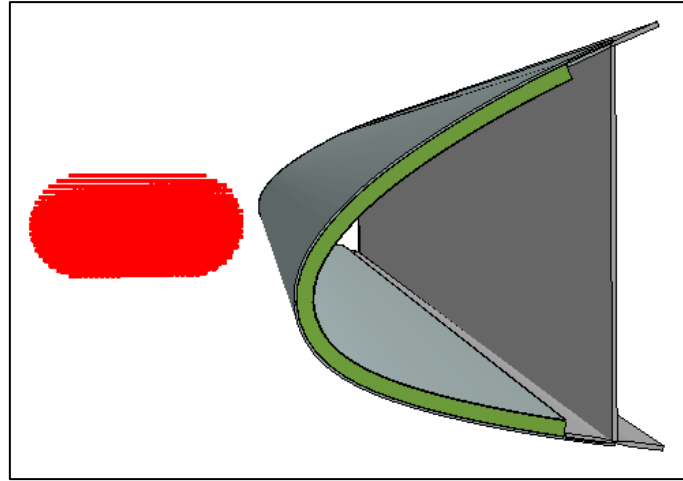
Figure 22. Honeycomb Sandwich Structure

Triangular Reinforcement Structures (TRS): This configuration is inspired from Liu's (2017) study, where triangular reinforcement structure is used. TRS reflects bird rather than absorb impact energy. Considering the weights, the traditional TRS is heavier than other configurations. Therefore, three different configurations were created for the triangular support structures. AA 2024 T3 is preferred for TRS in all different configurations.

The first configuration is traditionally designed triangular support structure. Different outer skin and TRS thickness values are examined for traditionally TRS configurations. The thicknesses satisfying CS-23 requirements and at minimum weight are listed in Table 5. TRS is shown in Figure 23.

Table 1. TRS Thickness Configurations

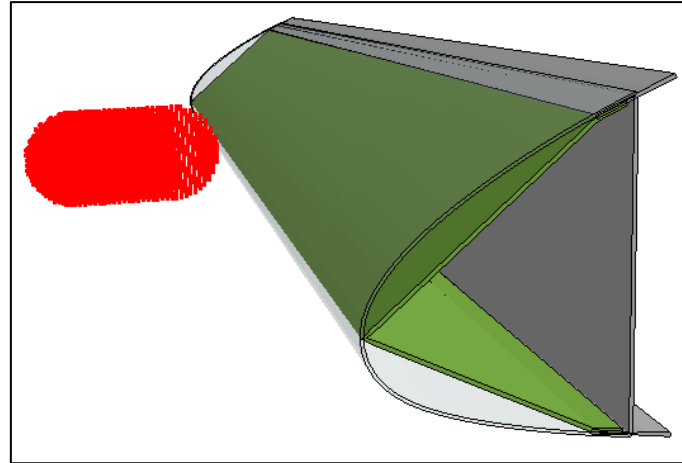| Configurations	Outer Skin Thickness	TRS Thickness
Traditional TRS-1	1 mm	1.05 mm
Traditional TRS-1.3	1.3 mm	0.85 mm
Traditional TRS-1.6	1.6 mm	0.58 mm

Figure 23. Traditional TRS

In the second configuration, regions showing low stress values under load conditions are removed from the structure. The thickness satisfying CS-23 requirements and at minimum weight are listed in Table 6. Topological TRS is shown in Figure 24.

Table 2. Topological TRS Thickness Configurations

Configurations	Outer Skin Thickness	TRS Thickness
Topological TRS 1	1 mm	1.75 mm
Topological TRS 1.6	1.6 mm	0.96 mm
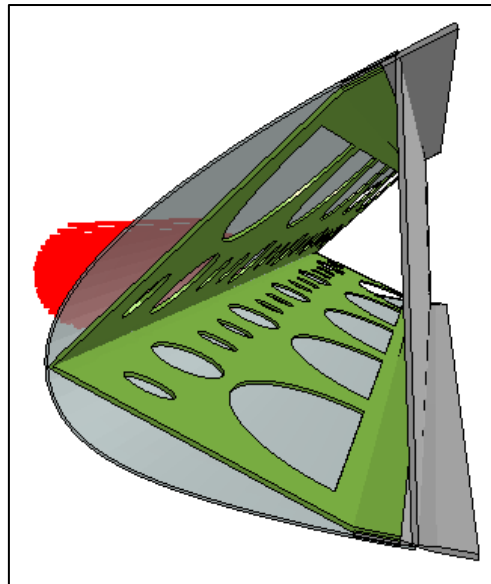
Figure 24. Topological TRS

In the third configuration, topometry study is carried out to reduce the thickness of TRS while maintaining its rigidity. In this configuration, stringers are added to prevent surface buckling. Topometric support structures are added to regions showing high stress values under load conditions on the structure. Topometric support structures have same thickness with TRS in all configurations. The thickness satisfying CS-23 requirements and at minimum weight are listed in Table 7. Topometric TRS is shown in Figure 25.

Table 3. Topometric TRS Thickness Configurations

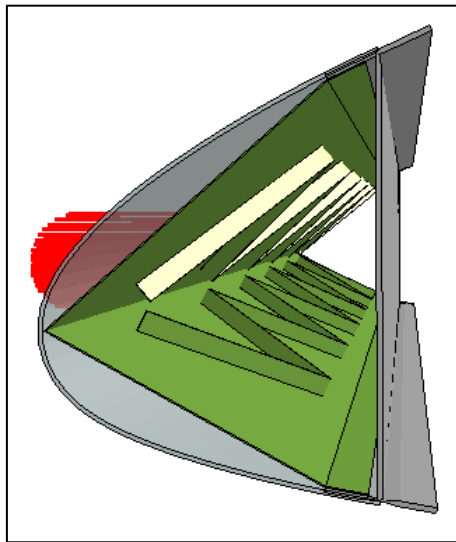| Configurations	Outer Skin Thickness	TRS Thickness
Topometric TRS 1	1 mm	0.875 mm
Topometric TRS 1.3	1.3 mm	0.75 mm
Topometric TRS 1.6	1.6 mm	0.4mm

Figure 25. Topometric TRS

Modified Structures: This configuration is inspired from Kumar's (2017) study, where modified structures are used. The modified structures are created by changing the structures and configurations of traditional support elements. The developed structures have three different configurations within themselves. AA 2024 T3 is used for all added support structures.

In the first configuration, sub spar element used for support structure. There are two side ribs and one sub spar in the configuration and sub spar is placed at 75 mm from the front spar. Outer skin and side rib thickness is 1 mm and sub spar thickness are determined as 2.5 mm. The modified structure with sub spar is shown in Figure 26.
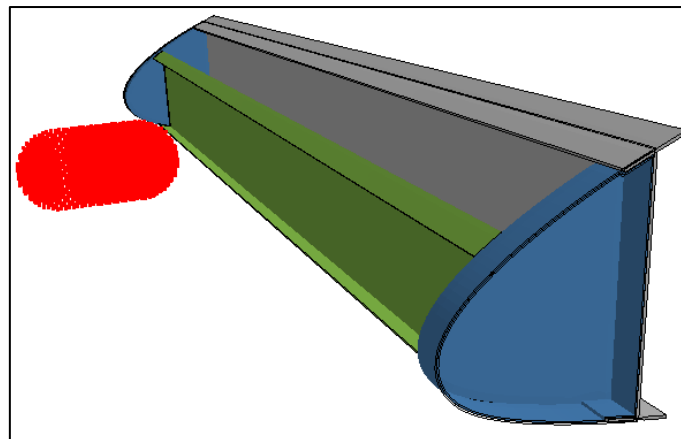

Figure 26. Modified Structure - Sub Spar Configuration

In the second configuration, 7 front ribs have been added in addition to the sub spar. Each rib is 125 mm apart from each other and 20 mm wide. The thickness of the outer skin, front ribs and side ribs is 1 mm, while the thickness of the sub spar is 1.75 mm. Thicknesses satisfying CS-23 requirements and at minimum weight are found. The modified structure with front ribs is shown in Figure 27.
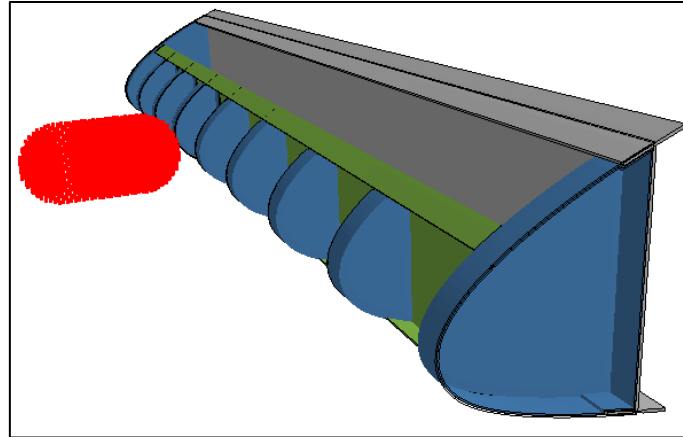

Figure 27. Modified Structure - Front Ribs Configuration

In the third configuration, eight ribs between fronts spar and sub spar were investigated. Each rear rib has 250 mm wide. Here, the thickness of outer skin, side ribs, front ribs and sub spar is expected as 1 mm. The modified structure with rear ribs is shown in Figure 28.
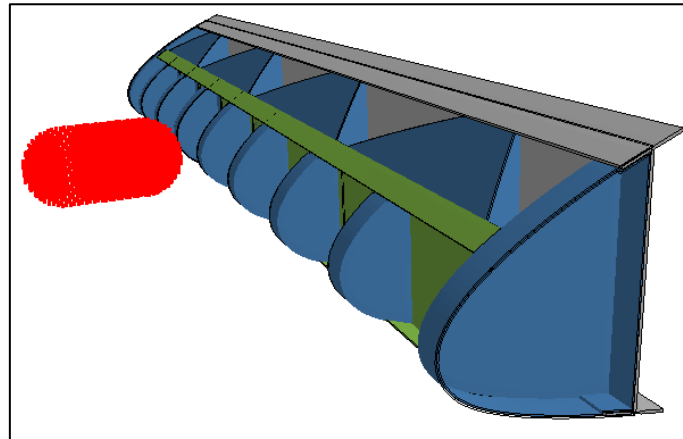

Figure 28. Modified Structure - Rear Ribs Configuration

Re-Entrant Honeycomb Structures: Negative Poisson's ratio (NPR) structures have been used as energy absorbent structures in various industries. [Wang, 2021]. Re-entrant honeycomb structure between the spar elements in the wing leading edge configuration has been created. When defining a cell dimensions, height size of the cell defined as 'h', edge length of the cell defined as 'l', edge thickness of the cell defined as 't' and 'alpha' parameters expressing the angle of the cell's edge to the vertical axis. In Figure 29, the parameters expressing the dimensions for the unit cell are shown.
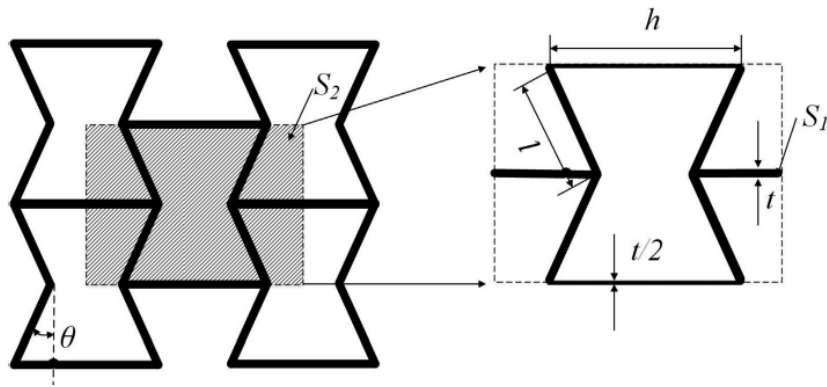
Figure 29. NPR Geometry

The NPR structure to be used on the wing leading edge consists of 3x3x31 cells. The lengths of the cell's height and the edge length are h = 20 mm and l = 10 mm, respectively. The thickness of the edge t = 1.2 mm. The cell - wall angle θ = 30 °. AA 2024 T3 was preferred for the NPR structure. A representative cell structure is shown in Figure 30.
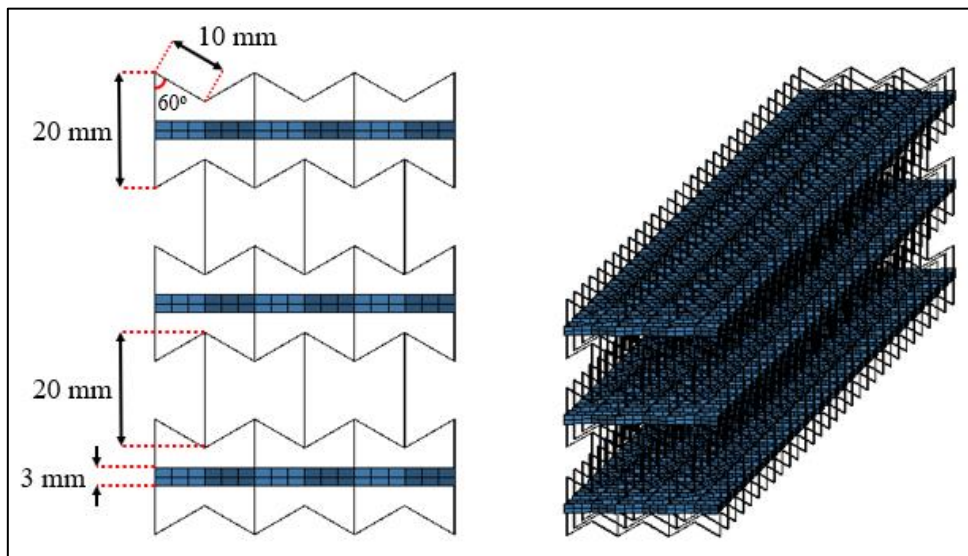

Figure 30. NPR Structure

In the configuration created with the NPR structure, the outer skin thickness is 1 mm, sub spar in the front is 0.7 mm, and the sub spar in the middle is 1.2 mm. Figure 31 shows the leading edge of the wing, with NPR structure.
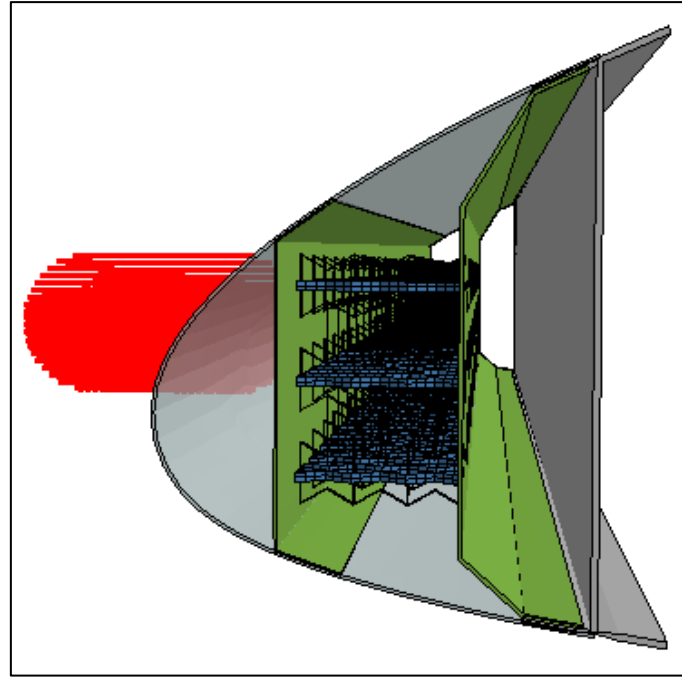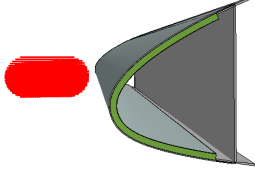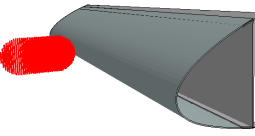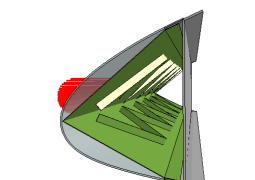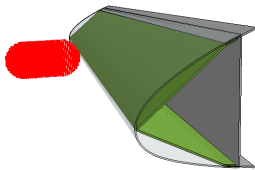
Figure 31. Leading Edge with NPR Structure

RESULTS

Table 8 shows the support structures with the best crash performance and their weights. Several thickness configurations have been analysed to find minimum weight satisfying CS-23 requirements. The order of the support structures in Table 8 is determined according to the first priority of meeting the impact requirements and the second priority of having the minimum weight. The followings are observed from Table 8:
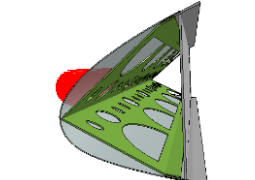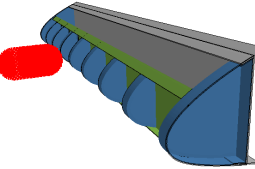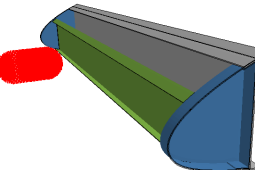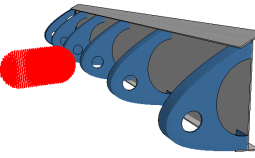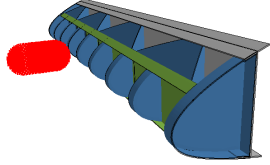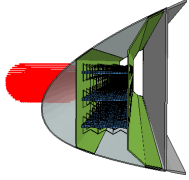
- The best performance is achieved when the honeycomb supporting structure is used.
- Interestingly, the second-best performance is achieved by the "Outer Surface Only" configuration with a thickness of 1.85 mm, resulting in 3.082 kg mass only.
- TRS 1 configurations show the best crash and weight performance among the TRS 1, 1.3 and 1.6 configurations; therefore, Table 8 includes only the 1 mm outer skin configurations.
- In the traditional rib design, two different configurations related to the collision zone are examined. Damage occurs to the front spar element because of the outer skin tearing during the impact in both configurations. The main reason for this behaviour is that the ribs behave rigidly and do not deform and absorb energy during collision.
- When thickness configurations for modified structure sub spar configuration are examined, the weight of the lightest structure that provides crash performance is 3.648 kg.
- Although the thickness of the support structures is increased in the modified structure with rear ribs configuration, it does not meet the collision requirements, even though the mass is 3.469 kg.
- When the crash performances of NPR structures are examined, depending on changing NPR and sub spar thicknesses, only the 1 mm outer skin configurations are observed to show better performance in all TRS configurations.

Table 4: The Support Structures that Satisfy the Requirements and Ranks

Rank	Support Structures		Total Weight (Kg)	EASA CS-23
1		Honeycomb	2.961	✔
2		Outer Surface Only	3.082	✔
3		Topometric TRS 1.0	3.103	✔
4		Traditional TRS 1.0	3.185	✔
5		Topological TRS 1.0	3.300	✔
6		Modified Structure Front Ribs Configuration	3.336	✔
7		Modified Structure Sub Spar Configuration	3.648	✔
-		Traditional Rib Design	3.418	✘

-		Modified Structure Rear Ribs Configuration	3.469	✗
-		NPR	3.788	✗

9. CONCLUSION

In this study, the effects of the bird strike to the leading edge of the wing of a training aircraft was investigated in accordance with EASA CS-23 standards. After performing validation of our bird and wing leading edge finite element models, we compared various design options for energy absorbing support structures (to be used in the leading edge geometry provided by TAI) in terms of their collusion and weight performances.

First of all, a design without support structure was considered, and the value of the outer skin thickness to protect against bird strikes on the leading edge was determined. The outer skin thickness of 1.85 mm was found to provide protection against bird strike and provides better weight performance than all designs with support structures except honeycomb support structure. It is noteworthy that the absence of any support structure on the wing should further be examined to determine whether it is suitable for flight, considering the different loads and vibration that may occur on the flight.

Amongst all support structures examined, honeycomb panel showed the best collusion and weight performance. Since support structures except honeycomb were examined, TRS variances performed well in terms of weight.

TRS were used to reflect bird rather than absorb impact energy at the time of collision. Among the configurations, while decreasing the outer skin thickness from 1.6 to 1 mm, increasing TRS thickness showed better performance. Topometric TRS showed the best results among TRS. It was observed that the topometric TRS maintained its rigidity during impact. Due to its rigidity, it created a knife effect on the bird at the time of collision. As the TRS thickness decreased in structures, the knife effect decreased although the TRS became lighter.

Modified structures were created with different combinations of traditional support structures. Since the modified structure are examined, energy absorbance values were increased depending on the thickness of the sub spar and outer skin. It was observed that the front ribs did not absorb energy during the impact and designs with rear ribs were not efficient absorbers.

NPR structures used in this study at the wing leading edge could not provide sufficient protection due to the presence of a narrow collision zone.

FUTURE WORK

Negative Poisson Ratio structures are among the structures frequently used in energy absorbing systems. With the developing production techniques, the effect of decreasing the unit cell size in the collision region and increasing the number of unit cells on the collision performance, such as a honeycomb sandwich panel in leading edge can be examined.

ACKNOWLEDGEMENTS

REFERENCES

Anghileri, M., Castelletti, L. M. L., & Mazza, V. (2005, May). Birdstrike: approaches to the analysis of impacts with penetration. In *International Conference on Impact Loading of Lightweight Structures, WIT Transactions on Engineering Sciences* (Vol. 49).

Arachchige, B., Ghasemnejad, H., & Yasaee, M. (2020). Effect of bird-strike on sandwich composite aircraft wing leading edge. Advances in Engineering Software, 148, 102839.

Barber, J. P., Taylor, H. R., & Wilbeck, J. S. (1975). Characterization of Bird Impacts on a Rigid Plate, Air Force Flight Dynamics Laboratory Technical Report. AFFDL-TR-75-5.

Belkhelfa, F. Z., & Boukraa, S. (2020). Damage prediction and test validation of bird impacts on aircraft leading edge's structures. *International Journal of Crashworthiness*, 1-18.

Castelletti, L. M., & Anghileri, M. (2003). Multiple Birdstrike Analysis–A survey of feasible techniques, 30th European Rotorcraft Forum. *Marseilles, Frances, September*, 14-162003.

Dede, O., & KAYRAN, A. (2015). Investigation of effects of bird strike on wing leading edge by using explicit finite element method.

Di Caprio, F., Cristillo, D., Saputo, S., Guida, M., & Riccio, A. (2019). Crashworthiness of wing leading edges under bird impact event. *Composite Structures*, *216*, 39-52.

Guida, M., Marulo, F., Meo, M., Grimaldi, A., & Olivares, G. (2011). SPH–Lagrangian study of bird impact on leading edge wing. *Composite Structures*, *93*(3), 1060-1071.

Guida, M., Moccia, A., & Marulo, F. (2008). *Study, Design and Testing of Structural, Configurations for the Bird-strike Compliance of Aeronautical Components*. CUEN.

Hanssen, A. G., Girard, Y., Olovsson, L., Berstad, T., & Langseth, M. (2006). A numerical model for bird strike of aluminium foam-based sandwich panels. *International journal of impact engineering*, *32*(7), 1127-1144.

Hedayati, R., & Sadighi, M. (2015). *Bird strike: an experimental, theoretical and numerical investigation*. Woodhead Publishing.

Hedayati, R., Sadighi, M., & Mohammadi-Aghdam, M. (2014). On the difference of pressure readings from the numerical, experimental and theoretical results in different bird strike studies. *Aerospace Science and Technology*, *32*(1), 260-266.]

Heimbs S, (2011) Computational methods for bird strike simulations: A review, Computers and Structures, 2011, 89(23-24), 2093-2112.

Johnson, A. F., & Holzapfel, M. (2003). Modelling soft body impact on composite structures. *Composite Structures*, *61*(1-2), 103-113.

Lavoie, M. A., Gakwaya, A., Ensan, M. N., Zimcik, D. G., & Nandlall, D. (2009). Bird's substitute tests results and evaluation of available numerical methods. *International Journal of Impact Engineering*, *36*(10-11), 1276-1287.

Liu, J., Li, Y., Yu, X., Tang, Z., Gao, X., Lv, J., & Zhang, Z. (2017). A novel design for reinforcing the aircraft tail leading edge structure against bird strike. *International Journal of Impact Engineering*, *105*, 89-101.

LSTC, Livermore Software Technology Corporation, LS-DYNA Theory Manual (2007).

McCallum, S. C., & Constantinou, C. (2005, May). The influence of bird-shape in bird-strike analysis. In *5th European LS-DYNA users conference, Birmingham*.

Metz, I. C., Ellerbroek, J., Mühlhausen, T., Kügler, D., & Hoekstra, J. M. (2020). The bird strike challenge. *Aerospace*, *7*(3), 26.

Nizampatnam, L., & Horn, W. (2008). Investigation of equation of state models for predicting bird impact loads. In *46th AIAA Aerospace Sciences Meeting and Exhibit* (p. 682).

Smojver, I., & Ivančević, D. (2010). Numerical simulation of bird strike damage prediction in airplane flap structure. Composite structures, 92(9), 2016-2026.

Wang, T., An, J., He, H., Wen, X., & Xi, X. (2021). A novel 3D impact energy absorption structure with negative Poisson's ratio and its application in aircraft crashworthiness. *Composite Structures*, *262*, 113663.